Journal of the Korean Physical Society
https://doi.org/10.1007/s40042-024-01237-x

Online ISSN 1976-8524
Print ISSN 0374-4884

ORIGINAL PAPER - PARTICLES AND NUCLEI

Construction of a new multi-reflection time-of-flight mass spectrograph at RAON

Jun Young Moon[1] · Peter H. Schury[2] · Michiharu Wada[2] · Yoshikazu Hirayama[2] · Hiroari Miyatake[2] · Yutaka X. Watanabe[2] · Hironobu Ishiyama[3] · Marco Rosenbusch[3] · Yuta Ito[4] · Aiko Takamine[5] · Toshitaka Niwase[5] · Hermann Wollnik[6] · Zeren korkulu[7] · Taeksu Shin[1] · Jinho Lee[1]

Received: 21 August 2024 / Revised: 29 October 2024 / Accepted: 5 November 2024

Abstract

A new large-scale heavy-ion accelerator complex, RAON (Rare isotope Accelerator complex for ON-line experiments), in Korea has implemented the state-of-art device, multi-reflection time-of-flight mass spectrometer (MRTOF-MS) for the mass spectrometry of the exotic nuclei. Using the multi-reflections of ions between a pair of grid-free mirror electrodes and therefore extending the fly length, it can achieve the incredibly high mass resolving power of $> 10^5$ within a short measurement time of < 10 ms, providing the nuclear mass of the exotic nuclei with a high-precision level of sub-ppm. The device is coupled to one of the beamlines in the ISOL experimental hall, ready for participating in the longstanding topics of nuclear structure in the outskirts of the nuclear chart and nucleosynthesis of heavy elements in explosive astrophysical environments. The exclusively high mass resolving power is also advantageous for reducing the isobaric contaminants that rare isotope ion beam facilities suffer from. In this paper, we present a summary of the construction and current performance of the RAON MRTOF-MS.

Keywords Nuclear mass · Time-of-flight · Multiple reflections · Radioactive ion beam · ISOL

1 Introduction

The atomic nucleus is a complex system of protons and neutrons, where the nuclear interaction plays a critical role in confining them in a finite quantum volume. Because of the interaction, equally the binding energy, the nucleus itself is slightly lighter than the sum of all nucleons, and therefore, the experimentally observed mass data can provide us with a probe to examine the interaction in the region far from the stability. From the differences in the binding energy within the isotonic to isotopic chains, it is possible to have clear evidence of the transition of the nuclear structure or shape as a function of proton number (isotonic chain) or neutron number (isotopic chain). Moreover, in the nucleosynthesis of heavy elements, the nuclear mass of atomic nuclei is a vital input for the abundance pattern reproduction using the network calculation, especially near the drip line, because it as an exponent primarily affects the reaction rate [1] or relative abundance at the waiting points [2].

Since the first successful extraction of radioactive ion beam (RIB) by the Isotope Separation On-Line (ISOL) method developed in the 1950s [3, 4], more advanced radioactive ion beam facilities have been constructed over the world, which are capable of producing more exotic ion beams and in turn bringing the nuclear physics community with unexplored land far from the stability [5–9]. When a new isotope is discovered, the nuclear mass is the initially

✉ Jun Young Moon
jymoon@ibs.re.kr

1 Institute for Rare Isotope Science, Institute for Basic Science, Daejeon 34000, Korea

2 Wako Nuclear Science Center, Institute of Particle and Nuclear Studies, High Energy Accelerator Research Organization (KEK), Wako, Saitama 351-0198, Japan

3 RIKEN Nishina Center for Accelerator-Based Science, Wako, Saitama 351-0198, Japan

4 Advanced Science Research Center, Japan Atomic Energy Agency, Ibaraki 319-1195, Japan

5 Department of Physics, Kyushu University, 744 Motooka, Nishi-ku, Fukuoka 819-0395, Japan

6 New Mexico State University, Las Cruces, NM 88001, USA

7 Center for Exotic Nuclear Studies, Institute for Basic Science, Daejeon 34126, Korea

Published online: 26 December 2024

measurable physical property, even in the case of extremely low production yield. To measure the mass of exotic nuclei produced by the RIB facility, a particular method must be properly chosen according to its lifetime. For the lifetime of the order of a millisecond or less, the Bρ-TOF spectrometer is preferred, which is faster but has lower relative precision. On the other hand, the Penning Trap Mass Spectrometer (PTMS) can provide exclusively high relative precision of the order of ppb but is applicable only for a longer lifetime of the order of second. The storage ring type spectrometer, isochronous or Schottky type mass spectrometer, can provide the mass data with the intermediate relative precision of sub-ppm for the isotopes in the lifetime of longer than 100 ms [10].

Proposed by H. Wollnik and M. Przewloka in 1990 [11], the concept of grid-free multi-reflection time-of-flight mass spectrometer (MRTOF-MS) has been successfully implemented in studying the nuclear mass of the short-lived and its performance has been drastically improved through huge efforts, as well. For instance, it was recently reported that the mass resolving power achieved became similar to that of the Penning trap [12, 13]. However, not only for the mass measurement, more radioactive ion beam facilities are adopting novel techniques but for the so-called isobar separation to improve the signal-to-noise ratio in other rare event measurements [14].

A new RI beam facility in Korea, the Rare isotope Accelerator complex for ON-line experiment (RAON), has completed its construction in 2021 [15], with a unique concept of being capable of providing more exotic isotope beams by combining two typical methods of the ISOL and IF methods. The so-called RAON MRTOF-MS is a twin of that installed in the KISS facility [16, 17], a miniaturized version of the SLOWRI MRTOF-MS [18], and has been developed at the KEK/WNSC (High Energy Accelerator Research Organization, Wako Nuclear Science Center). Its performance and productivity are well described in [19]. At the RAON ISOL facility, the radioactive ion beam is produced by impinging the high-intense proton beam on the thick solid target and ionizing through particular ionization techniques [20]. After extraction, it can be transported with relatively low energy of less than 60 keV. It should be noted that the beam energy must be decreased to less than 20 keV due to the insufficient stopping power of the gas cell placed before the MRTOF-MS. As for the application of the device, it will be utilized not only for the mass measurement of the exotic nuclei but also for improving the purity of the ion beam for others. In this publication, we briefly discuss the implementation, construction, and offline performance of the RAON MRTOF-MS.

2 Apparatus

The constructed MRTOF-MS system is illustrated in Fig. 1 with a photo taken from the experimental hall. As shown, it primarily composes a radio-frequency (RF) trap system and an MRTOF anaylzer. Additionally, to thermalize the transported ISOL ion beam with energy of $\leq$ 60 keV, a gas cell filled with helium buffer gas is installed with an RFQ ion

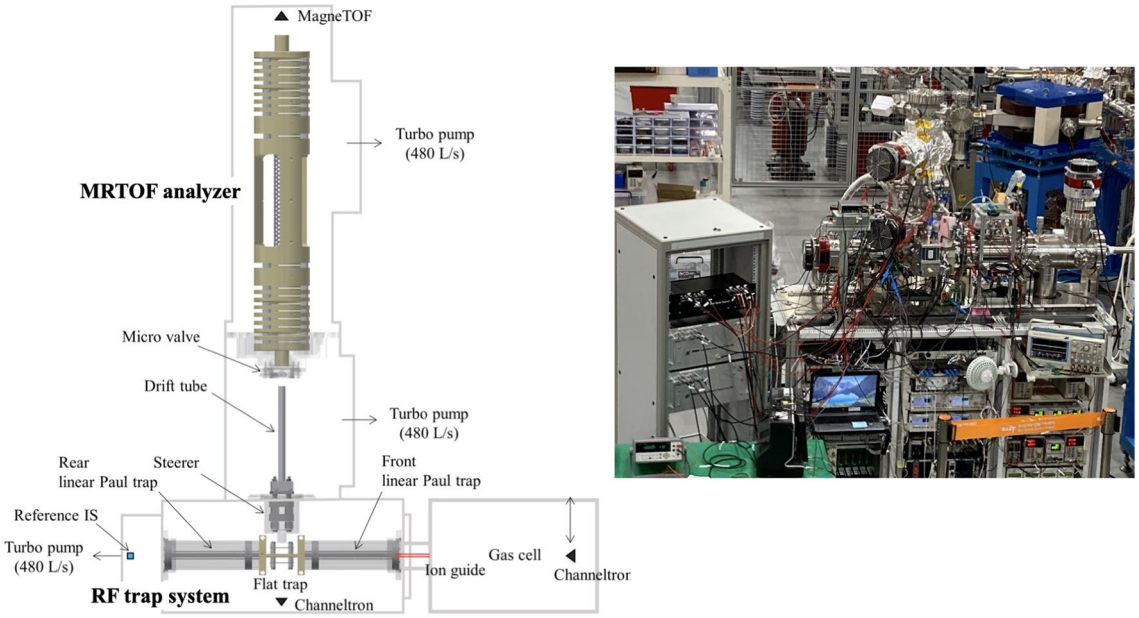

Fig. 1 Schematic view of the MRTOF-MS system (left) including the RF trap system, the ion guide (QPIG), additional ion optics (steerer, einzel lens), and MRTOF analyzer with a photo of its installation (right)

guide (quadrupole ion guide, QPIG). Using the MRTOF-MS and the gas cell enables us to stop the incident ISOL beams and to apply them for mass measurement and other applications such as beam diagnosis, which is useful for exploring the conditions to optimize ISOL beam production. And to minimize the impact of the helium buffer gas leaked from the gas cell on the vacuum upstream, a differential pumping section is placed between the gas catcher and the ISOL beamline. For ease of transport and maintenance, both of them are mounted on rails, and the entire system is placed on an aluminum frame with casters.

2.1 Principles of operation

Supposing that ions start with the same initial kinetic energy, the flight time for a given distance is solely proportional to the mass of the ions, i.e., $\propto \sqrt{m/q}$ for an ion of charge q, rest mass m. As presented in Fig. 2, in a specially designed potential distribution, ions that start with slightly different initial kinetic energy have different turning points, i.e., higher energy and further turning point, resulting in the temporal spread caused by the energy difference being minimized. However, it should be noted that the potential distribution must be shaped to construct laterally and longitudinal achromatic focusing conditions [11]. Such a special shape of the electrostatic potential distribution is created by carefully designing multiple electrodes of the analyzer and adjusting the potential of each of them. To minimize the phase space volume of the ions before multiple reflections, in the flat trap of the RF trap system, ions are cooled using dilute buffer gas and a bowl-shaped DC potential distribution and then ejected in a bunch form within a short period using a pulsed dipole electric field. The ejected ions are transferred through acceleration optics and two pairs of steerers installed immediately after the flat trap, optimizing the transmission rate and aligning the ion bunch with the optical axis of the MRTOF analyzer. To trap the delivered ions, two end-cap electrodes of the analyzer are switchable, as will be described in the later section. The injection end-cap electrode potential is switched to a sufficiently low even before the ions are ejected from the flat trap, and it is restored to its original value when the ions are near the ejection end-cap electrode. On the other hand, the ejection end-cap electrode potential is set to a lower potential when the ions complete a certain number of reflections and are ready to fly toward the external detector. In this system, the switch-off timing is mainly determined by two parameters, such as $a + b * \mathrm{n}$, where the a value, the b value, and n are the offset time, round-trip time, and number of reflections, respectively. By carefully choosing the a value, the ejection end-cap potential is lowered when the ion of interest travels the region far from the ejection end-cap electrode. Using this method, it is possible to increase the reflections of the ions, thereby extending the total flight length, and allowing very high mass resolving power.

2.2 RF trap system

The extracted ions from the gas cell are transported to the radio frequency (RF) trap system through the ion guide (QPIG). As illustrated in Figs. 3 and 4, it composes three Paul traps—two linear Paul traps (front and rear) and one flat trap.

The linear Paul trap (LPT) has four segmented parallel electrodes with rectangular cross-sections. Each electrode seems like a printed circuit board (PCB), with gold-plated copper printed on an insulator. On the backside, a signal distribution network consisting of resistors and capacitors couples all segments, allowing for the smooth supply of RF and DC voltage. The flat trap has a sandwich structure with two electrode plates facing each other. Each plate is also made by printing gold-plated copper electrodes on a Kapton insulator. More details of the flat trap are described in reference [21]. All DC and RF voltages are applied through driving circuit

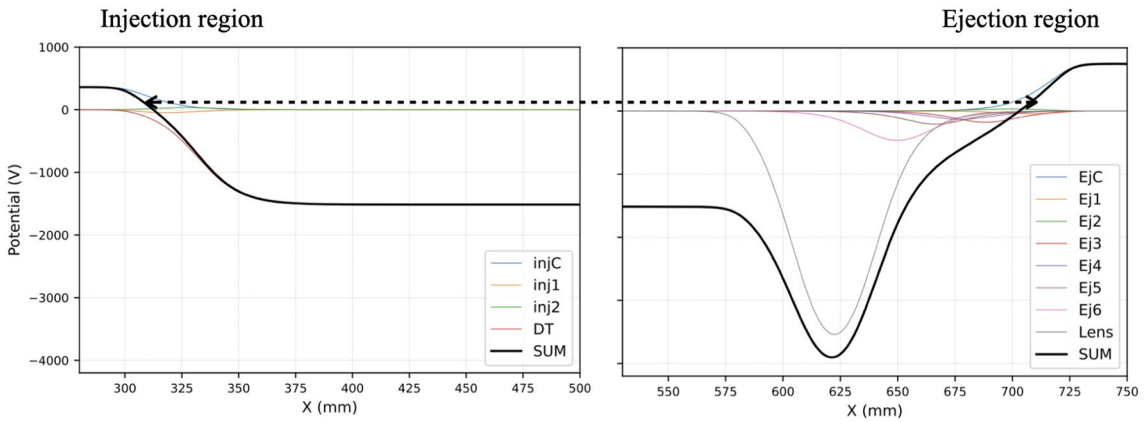

Fig. 2 Potential distribution, created by the voltages in Table 1: Dashed line represents the simplified ion path

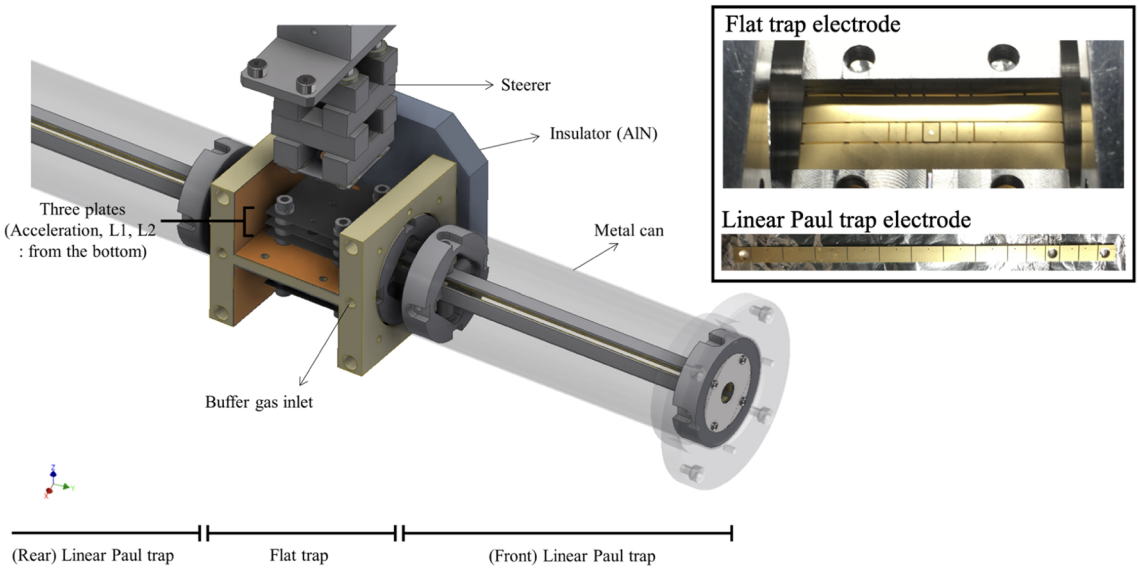

Fig. 3 3D drawing of the triple trap system (left) and photo of the electrode side (Right)

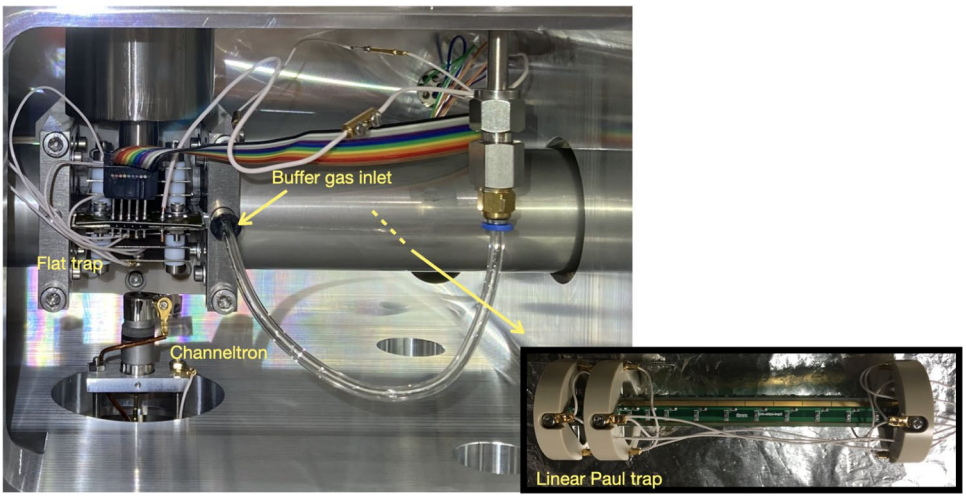

Fig. 4 Photo of the installed traps inside the chamber

boards, directly connected to the multi-pin feed-throughs. For the linear Paul traps, the unbalanced RF voltages, which are oscillated relative to the ground, are transformed into two balanced RF voltages with the same amplitudes but opposite phases using transformer-type BalUn coils on the driving circuit boards. However, the flat trap is supplied by unbalanced RF voltages. The resonance frequency can be varied using a variable condenser, and 2.5 MHz and 2.66 MHz are used for the linear Paul trap and the flat trap, respectively. The RF signals generated by the wave generators (4 ch, 33500B, Agilent Co.) are amplified by a 10W RF amplifier (5 ch, ZCA4040-IM10M5ch, RAD Co.).

The RF trap system needs sixteen (16) different DC voltage inputs, supplied by an in-house built 16-channel programmable DC power supply with $V_{out} < \pm 48$ V. A server software implemented in the Raspberry Pi mini PC there works to provide different voltage outputs as a function of time using TTL logic signals which are generated by an FPGA-base nano-sec time sequencer. The flexibility of the DC power supply allows for the use of the concomitant method [22], which is beneficial for ToF drift correction in the obtained spectrum.

Helium gas at low pressure is introduced into the inside flat trap to cool further the ions transported from the linear Paul trap. However, the pressure inside the trap is not possible to measure because of insufficient space for a pressure sensor, so a calculation using a commonly used tool, Molflow++, was carried out. As a result, the pressure inside the flat trap seems around three orders of magnitude higher than that of the trap chamber. The results are illustrated in Fig. 5.

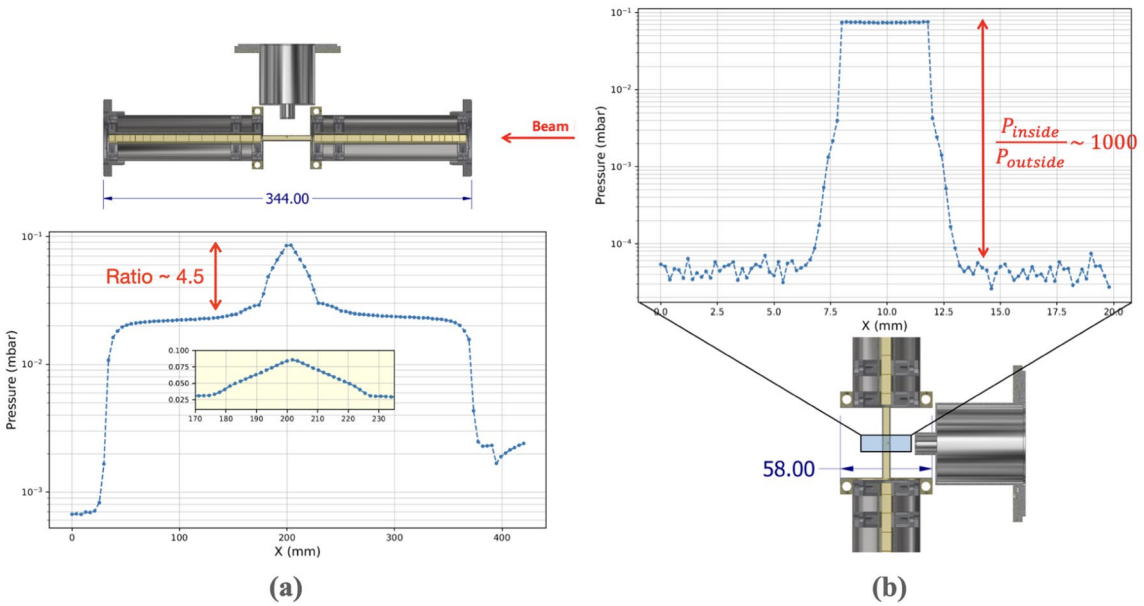

Fig. 5 Molflow++ calculation, showing the pressure inside the linear Paul trap (**a**) and the flat trap (**b**)

2.3 MRTOF analyzer

The MRTOF analyzer is the region where ions undergo oscillatory motion, and it is the most critical component for mass measurement utilizing the time-of-flight (ToF) technique. To describe the structure, it consists of multiple electrodes, as illustrated in Fig. 6, to create the specially designed electrostatic potential distribution. Nineteen (19) concentric and cylindrical electrodes of Au-plated aluminum are supported by stainless pillars and ceramic insulators, i.e., two switched end-cap electrodes (injection, ejection), two electrostatic mirrors, a central drift tube, and two lenses for radial confinement. A spacing of 1 mm between electrodes and small holes of $\phi 4$ mm in the two end-cap electrodes is designed to minimize the effect of the outside environment, such as the chamber potential and the detector bias on the shape of the potential shape which the ions undergo. The mirror electrodes have an inner diameter of 50 mm and an

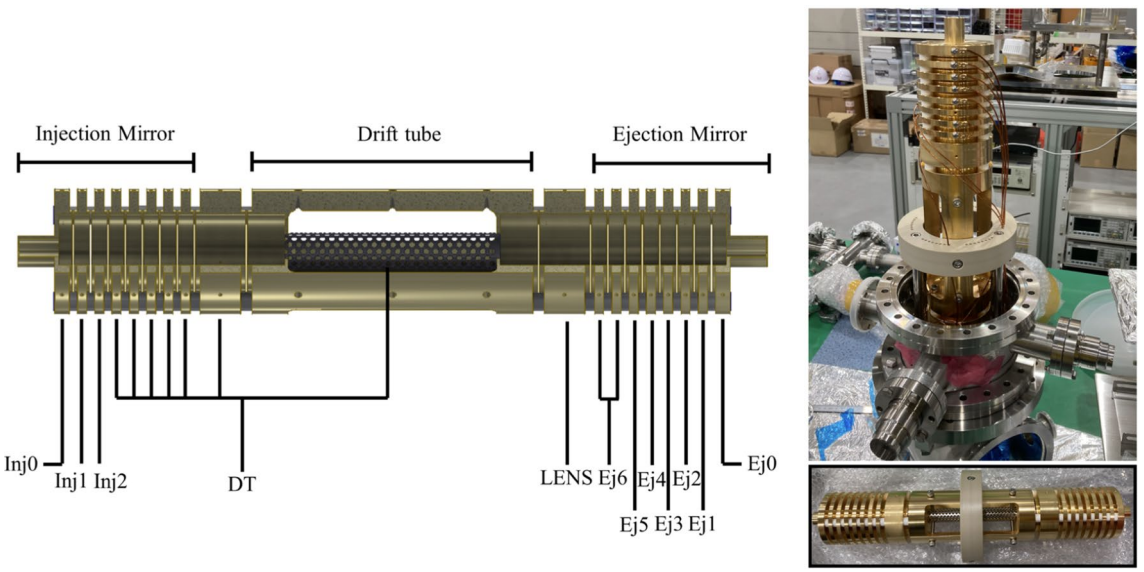

Fig. 6 3D drawing of the MRTOF electrodes and (left) and photo of its installation (right). Note that the outermost electrodes named by Inj0 and Ej0 are switchable by external triggers

outer diameter of 80 mm, while the drift tube is a long tube with a length of 137 mm, an inner diameter of 22 mm, and a thickness of 0.5 mm. The long metallic drift tube is designed to be sturdy and perforated, allowing for vacuum access from the outside. As a result, the total length is around a half meter (477 mm), a miniaturized version of the original SLOWRI MRTOF-MS design [18].

Kapton-coated wires are bolted to the electrodes, and voltages are supplied from external power sources through multi-pin feed-throughs. However, it should be noted that some of the inner mirror electrodes in the injection region are physically connected to the drift tube for asymmetric potential shape. In the ejection region, two innermost electrodes are connected by a wire inside. The detailed scheme of the wire connection and the name of each electrode are also illustrated in Fig. 6.

To maintain the delicate potential shape which is highly required for the high-precision measurement, the DC voltages are generated from the commercial multi-channel high-precision power supply modules (EHS 82-05X-K01, EHS 82-30x-K01, and EHS 82-60n, ISEG Co.), pass through the low-pass filter before the electrodes. The ISEG power supply modules adopted here and the circuit diagram of the filter are presented in Fig. 7. Adopting the RC filter allows better stabilization of voltages, but also brings disadvantages, especially for the usage of the switched end-cap electrodes. While the end-cap electrode bias potentials are switched with TTL logic signals, the actual voltage at the electrode might differ from that of the supply [13]. The electrode bias potentials applied in the offline commissioning with a thermal ion source of potassium are listed in Table 1 together with the specific information on the resistor and capacitor employed in each channel.

Table 1 Voltages applied to electrodes used in the offline measurement with a thermal ion source of potassium

Electrode	Voltage (V)	Remark
Trap+	135	
Trap-	– 35	
Acc	– 110	
L1	– 201	
L2	– 965	
PDT	– 963	
Inj0O	– 982	Open, 1 MΩ, 10 μF
Inj0C	362.4	Close, 1 MΩ, 10 μF
Inj1	– 194.3	10 MΩ, 1 μF
Inj2	124.9	10 MΩ, 1 μF
Inj3-7, inj-lens, drift tube	– 1514	5 MΩ, 1 μF
Lens	– 5080	
Ej6,7	– 892	10 MΩ, 1 μF
Ej5	– 732.4	5 MΩ, 1 μF
Ej4	– 469.5	10 MΩ, 1 μF
Ej3	– 631.2	5 MΩ, 1 μF
Ej2	116	5 MΩ, 1 μF
Ej1	– 183.82	5 MΩ, 1 μF
Ej0C	746.56	Close, 1 MΩ, 10 μF
Ej0O	– 380	Open, 1 MΩ, 10 μF

2.4 Control and data acquisition system

A control system is essential for the precise setting, monitoring, and optimization of the various parameters that influence system performance. Therefore, using a commercial platform builder, LabVIEW, a flexible control system is constructed, and communicates with the devices through TCP/IP. To operate important devices timely, the time sequencer, which as a critical component is in-house built, generates many TTL and NIM logic signals which are utilized for switching electrode potentials and as the start signal of a time-to-digital converter with the precision of ≥ 100 ps (TDC, MCS6A, FastCom Co.) [23]. The time sequencer is based on the Field Programmable Gate Arrays (FPGA), so its embedded program can be flexibly modified depending on the purpose. The simplified scheme in Fig. 8 shows the logic signals generated and their utilization in the MRTOF operation.

2.5 Vacuum system

The existence of the residual gas in the analyzer not only causes ion losses but also significantly affects the peak shapes in the TOF spectrum, simply due to collisions with residual gas atoms, while the ions oscillate. Due to the MRTOF analyzer being directly coupled to the flat trap which is filled with helium buffer gas, the intrusion of helium atoms into the analyzer chamber is inevitable. To mitigate the leakage of helium atoms from the flat trap encroaching into the analyzer chamber, a differential pumping section with narrow apertures is placed between the trap and the analyzer (See Fig. 1). A brief, but important investigation was performed, in which the pressure of the analyzer chamber was measured as the flat trap pressure was varied by adjusting the helium gas flow rate. From the result shown in Fig. 9, we found that the gas flow starts from the leakage valve position of 3.5 and significantly increases from 4.5. More importantly, the pressure of the analyzer shows an acceptably low pressure of $P_{mtof} = 1\times10^{-5}$ Pa when the trap pressure gauge indicates $P_{trap} = 3\times10^{-2}$ Pa. Note that the operation pressure region of the flat trap is around 2.2×10^{-2}Pa and the mean free path is around 1700 m, equally 1700 reflections of ion in the analyzer.

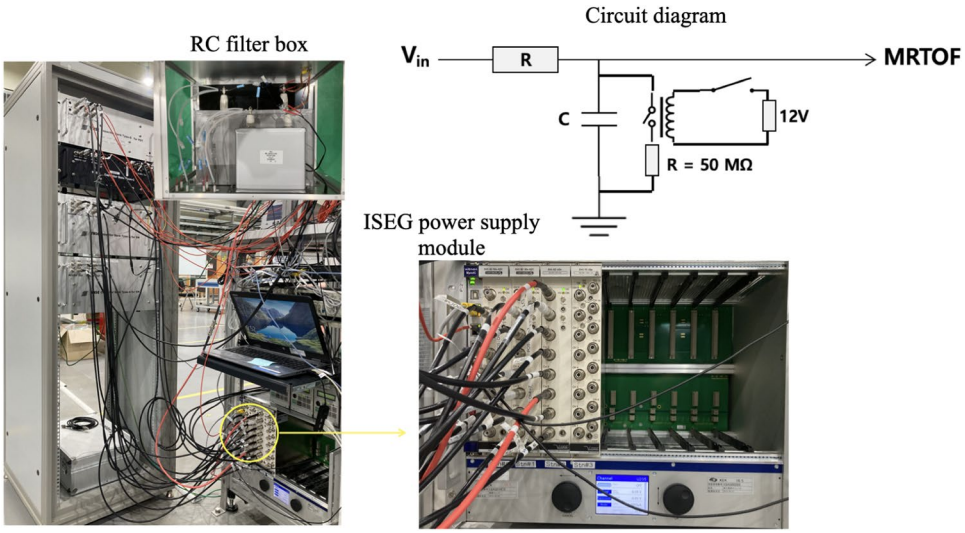

Fig. 7 Photo of the high-voltage power supply modules with a circuit diagram of the RC filter

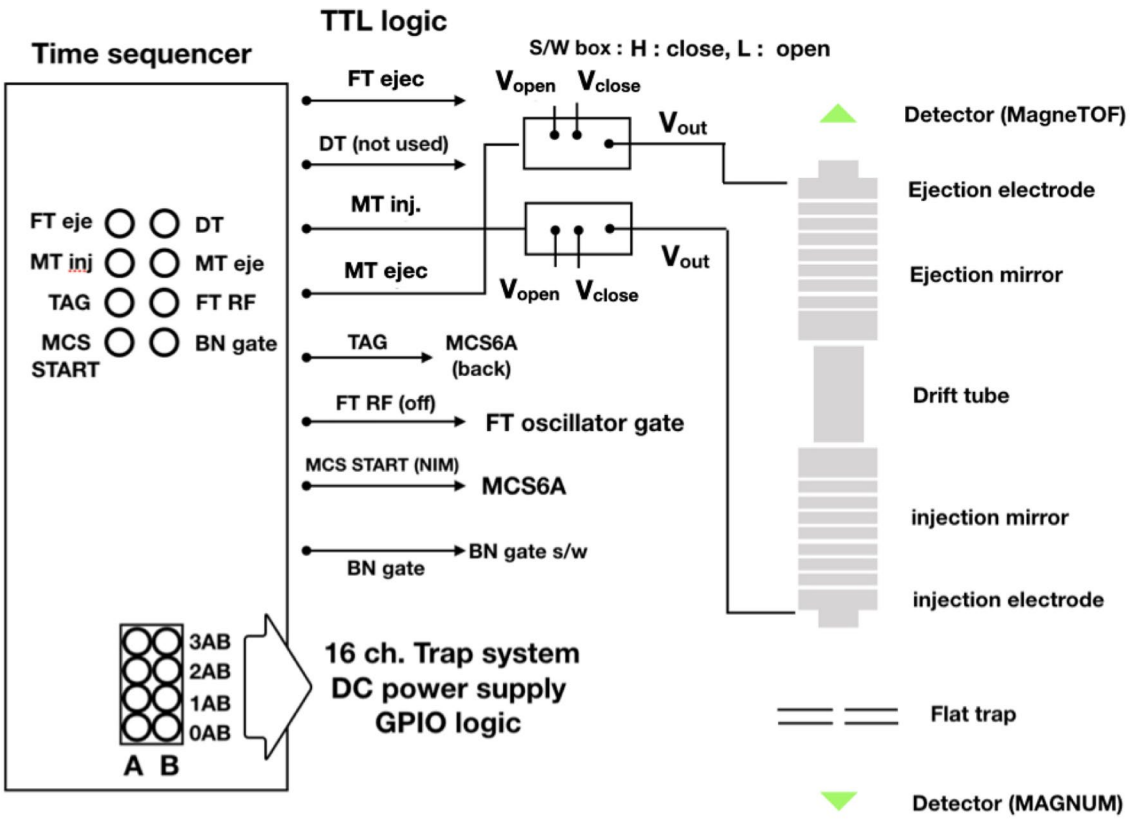

Fig. 8 Logic signals generated by the time sequencer and purposes. Note that only the MCS START is generated in the form of NIM logic

3 Performance test with offline ion source

After the completion of construction, the performance of each subsystem was examined using an alkaline ion source installed in the reference ion chamber. The potassium ion source (Heat Wave Labs.) can provide three K-isotopes (^{39}K−93.3%, ^{40}K−0.01%, and ^{41}K−6.73%), held by a structure located approximately 50 mm away from the entrance of the rear LPT. Its filament was heated by a high-current DC power supply (P4K-80 L, Matsusada Co.) to generate ions. Note that the power supply was floated at a certain potential (V_{anode}) to accelerate the emitted ions. For the detection of ion bunches after the

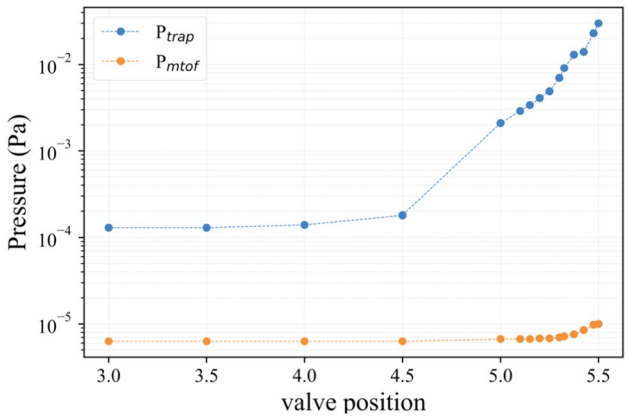

Fig. 9 Comparison of the pressures of the trap chamber and the MRTOF-MS region, measured as a function of gas flow rate

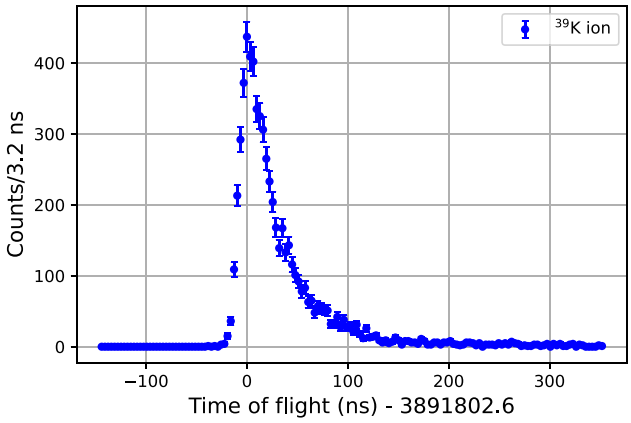

Fig. 10 An example of TOF spectrum of ^{39}K ions obtained at the higher laps, here at n = 350 laps

analyzer, a sub-nanosecond Time-of-Flight (ToF) detector, MagneTOF (Model 14925, ETP), was installed after the ejection end-cap electrode. Using the observed ion intensity, the optimization of all devices along the path to the detector was carried out. To efficiently transport ions toward the flat trap, the initial task involved tuning all relevant parameters, including the ion source potential, DC potentials, and RF parameters of the rear LPT. It was observed that the potentials of the outermost electrode of the rear LPT and the ion source were more sensitive. Following that, the parameters of the flat trap and the ion optics (three plates, steerer, drift tube, and microvalve) were finely tuned. After optimizing ion transport, we proceeded to tune the voltages of the MRTOF analyzer electrodes to achieve a mass resolution of over 100,000. Following that a and b values have been measured, we tried to find the so-called time focus by varying the number of reflections and analyzing the width of each TOF spectrum of ions acquired ('i-scan'), at which the width becomes minimized ('Isochronous'). Once the time focus was found, it was necessary to shift it toward the higher revolution number through adjustment of the voltages of the outermost electrodes (Inj0C and Ej0C in Table 1) and the drift tube. An example of TOF spectrum obtained from the measurement is presented in Fig. 10, which was in the case of n = 350 laps. Figures 11 and 12 illustrate the results of tuning for the case of potassium ion (^{39}K). From the i-scan, as shown in Fig. 11, we found that the time focus has occurred at n = 350 reflections, providing the mass resolving power of 110,000 (FWHM). At each measurement, the ToF spectrum was analyzed with a hybrid type of the exponential Gaussian function [24]. However, to investigate the magnitude of ion loss occurring during the reflections, the ion intensity as a function of the number of reflections was also measured. The measurement was performed from n = 100–510 with a step size of 10

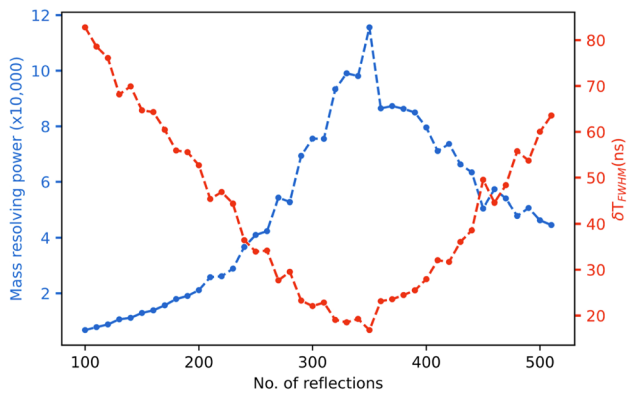

Fig. 11 Result of the i-scan for ^{39}K ions, where the blue dashed point line represents the mass resolving power as a function of the number of reflections, while the red one is the ToF width

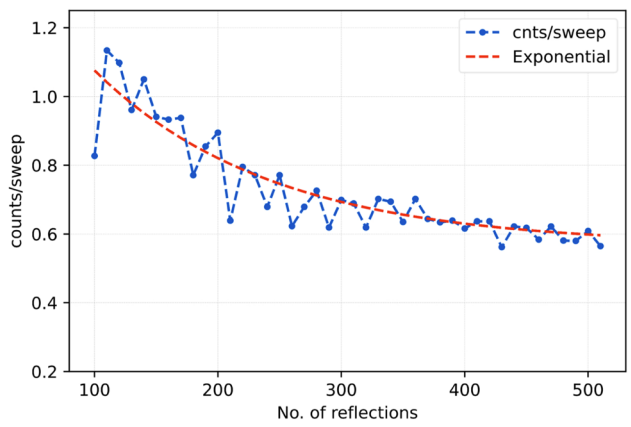

Fig. 12 Ion intensity of ^{39}K ions as a function of the number of reflections. For the comparison, the fitting result done by the exponential decay function is added (red dashed line)

laps, as illustrated in Fig. 12. The result indicates that the ion intensity, initially having 1.2 ions/sweep at $n = 100$, decays as a function of the reflection number with some fluctuation, approaching a saturation value of 0.56 ions/sweep. The pronounced decrease before $n = 200$ probably originates from a relatively large initial emittance of the ion cloud when it is ejected, compared to the acceptance of the MRTOF analyzer. The periodic fluctuation is more likely to be related to the angular misalignment between the trap and the MRTOF analyzer, so it could be minimized by adjusting the steering optics as suggested in [16].

4 Summary and outlook

The new multi-reflection time-of-flight mass spectrograph has been introduced at the RAON ISOL facility, constructed through collaboration between IBS/IRIS and KEK/WNSC. The MRTOF-MS system is a state-of-the-art, high-precision mass measurement device, offering the nuclear physics community enhanced opportunities to study the nuclear mass of short-lived isotopes. Rigorous checking with an offline ion source confirmed the functionality of all relevant systems, resulting in a typical mass resolving power of R_m ~100,000 and a short measurement time of approximately less than 10 milliseconds. During the system verification, we identified several issues, such as an asymmetric time-of-flight (ToF) peak shape with a longer slow tail and a relatively low ion survival probability under multiple reflections. We are optimistic that the entire system will be improved with further efforts. In addition, to extend the instrument's application, the isobar separation for other physics measurements requiring ion beams with minimal contaminants is being considered.

Acknowledgements The authors would like to express gratitude to the RAON ISOL facility staffs for their support of construction and offline measurements. This work was supported by the Institute for Basic Science (IBS-I001-D1) and the National Research Foundation of Korea (NRF) funded by the Ministry of Science and ICT (2013M7A1A1075764), Republic of Korea.

Declaration

Conflict of interest The authors declare that they have no conflict of interest.

References

1. H. Schatz, Int. J. Mass Spectrom. **349–350**, 181 (2013)
2. M.R. Mumpower, R. Surman, D.-L. Fang, M. Beard et al., Phys. Rev. C **92**, 035807 (2015)
3. O. Kofoed-Hanson, K.O. Nielsen, Phys. Rev. **82**, 96 (1951)
4. O. Kofoed-Hanson, K.O.N. Kongl, Danske Vidensk. Selsk. Mat.-Fys. Medd. **26**, 7 (1951)
5. Y. Blumenfeld, T. Nilsson, P. Van Duppen, Phys. Scr. **152T**, 014023 (2013)
6. R. Anne, D. Bazin, A. Mueller, J. Jacmart, M. Langevin, Nucl. Instr. Methods Phys. Res. Sect. A **257**, 215 (1987)
7. H. Geissel, P. Armbruster, K. Behr, A. Brundle, K. Burkard, M. Chen et al., Nucl. Instr. Methods Phys. Res. Sect. B **70**, 286 (1992)
8. H. Wei, H. Ao, S. Beher, N. Bultman, F. Casagrande, J. Chen, et al., Advances of the FRIB project. In 14th International Conference on Heavy Ion Accelerator Technology (2019)
9. T. Kubo, M. Ishihara, N. Inabe, H. Kumagai, I. Tanihata, K. Yoshida et al., Nucl. Instr. Methods Phys. Res. Sect. B **70**, 309 (1992)
10. B.H. Sun, Yu.A. Litvinov, I. Tanihata, Y.H. Zhang, Front. Phys. **10**, 102102 (2015)
11. H. Wollnik, M. Przewloka, Int. J. Mass Spectrom. Ion Proc. **96**, 267 (1990)
12. I. Mardor, A. Andres, T. Dickel et al., Phys. Rev. C **103**, 034319 (2021)
13. M. Rosenbusch, M. Wada, S. Chen, A. Takamine et al., Nucl. Instr. Methods Phys. Res. Sect. A **1047**, 167824 (2023)
14. F. Wienholtz, S. Kreim, M. Rosenbusch, L. Schweikhard, R.N. Wolf, Int. J. Mass Spectrom. **427**, 285 (2017)
15. B. Hong, AAPPS Bull. **33**, 3 (2023)
16. P. Schury, M. Wada, Y. Ito, F. Arai, S. Naimi, T. Sonoda, H. Wollnik, Nucl. Instr. Methods Phys. Res. Sect. B **335**, 39 (2014)
17. S.C. Jeong, N. Imai, H. Ishiyama, Y. Hirayama, H. Miyatake, Y.X. Watanabe, KEK Rep. 2010-2 (2010)
18. M. Rosenbusch, M. Wada, P. Schury, Y. Ito et al., Nucl. Instr. Methods Phys. Res. Sect. A **463**, 184 (2020)
19. T. Niwase, Y.X. Watanabe, H. Ishiyama, M. Mukai, P. Schury et al., Phys. Rev. Lett. **130**, 132502 (2023)
20. J. Lee, H.-J. Yim, T. Hashimoto, Y.H. Park et al., Nucl. Instr. Methods Phys. Res. Sect. B **542**, 17 (2023)
21. Y. Ito, P. Schury, M. Wada, S. Naimi et al., Nucl. Instrum. Method B **317**, 544 (2013)
22. P. Schury, Y. Ito, M. Rosenbusch, H. Miyatake et al., Int. J. Mass Spectrom. **433**, 40 (2018)
23. Fast ComTec GmbH, https://www.fastcomtec.com/ufm/mcs6a
24. K. Lan, J.W. Jorgenson, J. Chromato. **915**(1–2), 1 (2001)